

Photodissociation spectroscopy of the dysprosium monochloride molecular ion

Alexander Dunning,^{1, a)} Alexander Petrov,^{2, b)} Steven J. Schowalter,¹ Prateek Puri,¹ Svetlana Kotochigova,² and Eric R. Hudson¹

¹⁾*Department of Physics & Astronomy, University of California, Los Angeles, CA 90095, USA*

²⁾*Department of Physics, Temple University, Philadelphia, PA 19122, USA*

We have performed a combined experimental and theoretical study of the photodissociation cross section of the molecular ion DyCl^+ . The photodissociation cross section for the photon energy range $35,500\text{ cm}^{-1}$ to $47,500\text{ cm}^{-1}$ is measured using an integrated ion trap and time-of-flight mass spectrometer; we observe a broad, asymmetric profile that is peaked near $43,000\text{ cm}^{-1}$. The theoretical cross section is determined from electronic potentials and transition dipole moments calculated using the relativistic configuration-interaction valence-bond and coupled-cluster methods. The electronic structure of DyCl^+ is extremely complex due to the presence of multiple open electronic shells, including the $4f^{10}$ configuration. The molecule has nine attractive potentials with ionically-bonded electrons and 99 repulsive potentials dissociating to a ground state Dy^+ ion and Cl atom. We explain the lack of symmetry in the cross section as due to multiple contributions from one-electron-dominated transitions between the vibrational ground state and several resolved repulsive excited states.

I. INTRODUCTION

Molecular ions provide a platform for many advances in quantum physics and chemistry¹. They offer the same rich rovibrational structure and internal fields as their neutral counterparts, yet they are more straightforward to trap on long timescales, and they offer the potential for improved quantum coherence². These advantages have motivated many recent research efforts centered around molecular ions, including studies of the time-variation of fundamental constants³, searches for the electric dipole moment of the electron^{4,5}, and designs of quantum computing architectures in which molecular ion qubits are addressed by microwave² and laser⁶ fields. Necessarily, much progress has been made toward cooling molecular ions to quantum degeneracy: millikelvin translational temperatures and Coulomb crystallisation have been demonstrated with hydride-like⁷ and more complex⁸ molecular ions via sympathetic cooling of the molecular species by co-trapped laser-cooled atomic ions; and quenching of the rotational and vibrational motion of molecular ions has been achieved through sympathetic cooling by a cryogenic buffer gas⁹, and by a co-trapped cloud of ultracold neutral atoms¹⁰, respectively.

However, since the field of ultracold molecular ion physics is relatively young, one significant obstacle to progress in these experiments is the small pool of available spectroscopic data. In the past three decades, there have been relatively few experimental spectroscopic studies of diatomic molecular ions (see Saykally and Woods' summary of pre-1980 work in Ref. 11, and as a representative yet non-exhaustive list of the work since then, see Refs. 12–21).

In this report we present spectroscopic data, and a detailed theoretical discussion, of the molecular ion DyCl^+ , which is an interesting candidate for molecular laser cooling, ultracold chemistry in atom-ion systems, and in the long-term, scalable quantum computing. The interest in DyCl^+ , and indeed the lanthanide halides in general, stems from the notion that unpaired electrons in the $4f$ core of the lanthanide element play little or no part in the bonding of the molecular system²². Since excited states within the $4f$ levels are often present at optical intervals, and Laporte-forbidden $f-f$ transitions may be activated by vibrations and interactions with the ligand²³, this could give rise to optically addressable transitions with highly diagonal Franck-Condon factors.

Owing to a heightened complexity, theoretical approximations regarding core electron configurations and molecular potentials in the lanthanide halides remain contestable. Demonstrating agreement between experiment and theory will naturally help to strengthen the validity of our chosen theoretical methods.

The remainder of this manuscript is structured as follows. In Sec. II, we describe the theoretical calculations of the DyCl^+ molecular potentials, along with predictions of transition strengths between bound and repulsive states. In Sec. III, we outline the experimental methods for measuring the photodissociation cross section. We present a comparison of our theoretical and experimental results in Sec. IV, along with some discussion regarding bound excited state potentials in the molecular ion, before summarising in Sec. V.

II. THEORETICAL CALCULATIONS

The DyCl^+ molecule is a truly relativistic molecule with an intricate electronic structure, whose complexity is due to a partially-filled Dy^+ anisotropic inner $4f^{10}$ shell, which lies beneath an open $6s$ shell. In fact, the ground state of the Dy^+ ion has a very large total angular

^{a)}Electronic mail: alexander.dunning@gmail.com

^{b)}Alternative address: NRC ‘Kurchatov Institute’ PNPI 188300, Division of Quantum Mechanics, St. Petersburg State University, 198904, Russia

j_1	j_2	$E/(hc)$ (cm^{-1})	Ω											
			10	9	8	7	6	5	4	3	2	1	0	
17/2	3/2	0.0	1	2	3	4	4	4	4	4	4	4	4	4
15/2	3/2	828.314	1	2	3	4	4	4	4	4	4	4	4	4
17/2	1/2	882.3515	1	2	2	2	2	2	2	2	2	2	2	2
15/2	1/2	1710.6655	1	2	2	2	2	2	2	2	2	2	2	2

TABLE I. The number of relativistic Hund’s case (c) potentials with label Ω for the energetically-lowest four dissociation limits of $\text{Dy}^+[4f^{10}(^5\text{I}_8)6s_{1/2}(8,1/2)_{j_1}] + \text{Cl}[3p^5(^2\text{P}_{j_2})]$, where j_1 and j_2 are the total angular momentum quantum numbers of Dy^+ and Cl, respectively [The ‘(8,1/2)’ notation indicates the core and outer total electronic angular momenta in the j-j coupling regime]. Here h is Planck’s constant and c is the speed of light.

momentum $j = 17/2$ (excluding nuclear spin) indicative of strong alignment of its electron spins. Coupling the Dy^+ ion with the Cl atom, which has an open $3p^5$ shell, makes the molecular structure even more complex.

In our dissociation experiment with photon energies around $40,000 \text{ cm}^{-1}$, we need only consider transitions between relativistic potentials that dissociate to the energetically-lowest four limits of $\text{Dy}^+(4f^{10}6s) + \text{Cl}(3p^5)$. The atomic states and energies of these limits are given in Table I. The angular momentum coupling of the DyCl^+ molecule is described by the Hund’s case (c) coupling scheme and labeled by Ω , the absolute value of the projection of the total electronic angular momentum $\vec{j} = \vec{j}_1 + \vec{j}_2$ on the intermolecular axis. Here \vec{j}_1 and \vec{j}_2 are the total atomic angular momenta of Dy^+ and Cl, respectively. Table I shows the number of potentials for each Ω yielding a total of 108 potentials.

We have determined the DyCl^+ potentials, for the bound and repulsive states corresponding to the configurations given in Table I, as a function of internuclear separation R , based on a two-step approach. First, we calculate relativistic potentials with a relativistic configuration-interaction valence-bond (RCI-VB) method²⁴ using a relatively small basis set limited by computational resources. In the RCI-VB method the molecular wave function is constructed from atomic Slater determinants with localized one-electron orbitals found by numerically solving the Dirac-Fock (DF) equation for occupied orbitals and DF or Sturmian equations for virtual or unoccupied orbitals. We perform all-electron calculations where, in principle, the dynamics of each electron is accounted for. To restrict the size of the Hamiltonian, excitations from the closed shells of Dy^+ are not allowed, while excitations of electrons in the open $4f^{10}$ and $6s$ shells and into unoccupied $6p$ and $5d$ virtual shells are allowed. These four shells form the active space of Dy^+ . Similarly, for the Cl atom, shells up to $2p$ remain closed while excitations of the occupied $3s$ and $3p$ shells into the virtual $3d$ and $4s$ are included.

Our calculations show that there are nine ionically-bonded attractive potentials, one for each $\Omega = 0$ up to

8, with splittings that are much less than their depth. The $\Omega = 8$ potential is the deepest. The remaining 99 potentials are repulsive or barely attractive. We denote the potentials by $V_{n,\Omega}^{\text{VB}}(R)$, where $n = 1, 2, 3 \dots$ labels the Ω potentials with increasing energy, and uniformly shift all potentials such that the energetically-lowest potential approaches zero energy in the limit of large separation.

The structure of the molecular potentials can be qualitatively understood by noting that when the $6s$ valence electron of Dy^+ is transferred to Cl, the ionically-bonded and thus the deeply-bound molecule $\text{Dy}^{++}\text{Cl}^-$ is formed. In this molecule, the Cl^- has a closed $3p^6$ shell, while Dy^{++} only has one open electron shell, the $4f^{10}$, with total angular momentum $j = 8$. Consequently, we have nine deep potentials, one for each projection quantum number $\Omega = 0$ to 8.

Next, we improve the nine attractive potentials with the help of *non-relativistic* coupled-cluster calculations, where we can include more electron-electron correlations with much larger basis sets as long as a single determinant dominates the bond, and with the realization that (small) splittings between potentials converge more rapidly than the absolute binding energy. We, therefore, compute the only non-relativistic potential consistent with $\Omega = 8$, corresponding to the Dy^{++} “stretched-state” with total electron spin $S = 2$ and projection of the electron orbital angular momentum $\Lambda = 6$ using single, double, and perturbative triple excitations (CCSD(T)). The coupled-cluster method does not converge for $\Omega < 8$ as then multiple determinants control the bonding.

For Dy we use the scalar relativistic Stuttgart ECP28MWB pseudopotential and associated atomic basis sets $(14s13p10d8f6g)/[10s8p5d4f3g]$ ²⁵. The basis set $\text{def2-QZVPP } (20s14p4d2f1g)/[9s6p4d2f1g]$ is used for Cl²⁶. The core electrons $1s^22s^22p^6$ for Cl and $4s^24p^64d^{10}$ for Dy are not correlated, leaving core-valence electrons of $3s^23p^5$ in Cl and $5s^25p^64f^{10}$ in Dy correlated. We find that the potential, $V^{\text{CC}}(R)$, has a minimum at $R_e = 4.63a_0$ with depth $D_e/(hc) = 32508 \text{ cm}^{-1}$ and where a_0 is the Bohr radius. For $^{161}\text{Dy}^{35}\text{Cl}^+$ it has a $\omega_e/(hc) = 441 \text{ cm}^{-1}$ and 120 bound states. Unsurprisingly, we find that $V^{\text{CC}}(R)$ is deeper than any of the relativistic potentials. Again this potential is shifted such that it approaches zero at large R . Finally, we construct $V_{n,\Omega}(R) = V^{\text{CC}}(R) + (V_{n,\Omega}^{\text{VB}}(R) - V_{1,8}^{\text{VB}}(R))$ for the nine attractive Ω potentials. The potential-energy functions for remaining mainly-repulsive electronic states are taken from the RCI-VB calculation.

The minima of the nine adjusted attractive potentials as well as the repulsive potentials relevant for the simulation of our photodissociation experiment are shown in Fig. 1. In addition, Table II shows the first thirty $J = 8$ vibrational energies of the ground state $n, \Omega = 1, 8$ or X potential for two isotopes of DyCl^+ .

In our experiment, we estimate the internal blackbody redistribution rate to be around 1 Hz, and so we predict that the molecules are approximately in rovibronic thermal equilibrium with the surroundings when photodis-

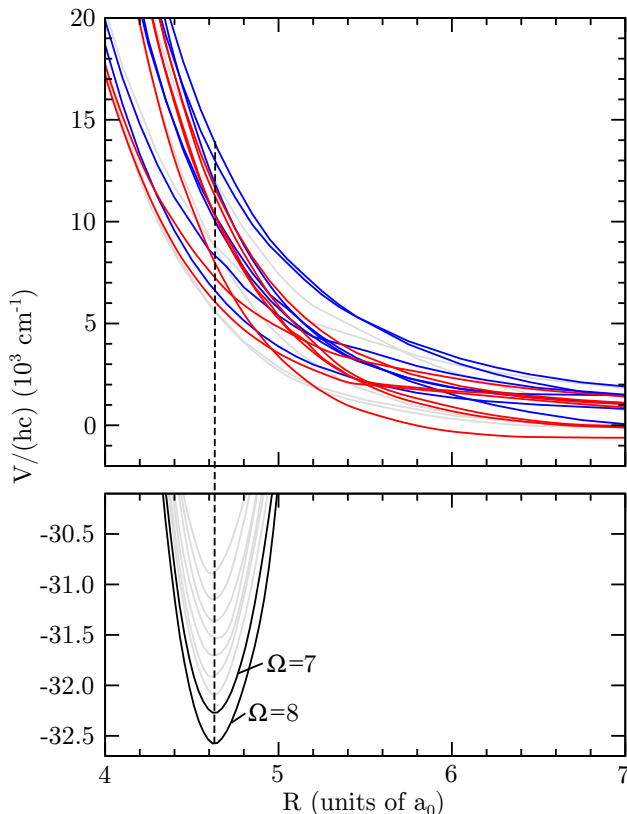


FIG. 1. (color online) Potential energy curves of the DyCl^+ molecule as a function of R . The bottom panel shows the nine attractive, deeply-bound potentials, one for each Ω from 0 to 8. The two black curves correspond to the $\Omega = 8$ and 7 potentials populated in our photodissociation experiment. Other potentials are shown by grey lines. The top panel shows repulsive and weakly-bound $\Omega' = 6, 7, 8,$ and 9 potentials. The seven red curves are $\Omega' = 7, 8,$ and 9 potentials with a large transition dipole moment to the $\Omega = 8$ ground state and dissociate to $\text{Dy}^+ + \text{Cl}$ limits. The other seven blue curves are $\Omega' = 6, 7,$ and 8 potentials that have a large transition dipole moments with the ground $\Omega = 7$ state. Other potentials are shown with grey lines. The dashed black line indicates vertical transitions from the $v = 0$ rovibrational level of the $\Omega = 8$ potential to repulsive potentials driven by one-color laser radiation.

sociation begins after 1.7 s of trapping. This approximation is validated by previous studies of molecular ions with more straightforward electronic structure using the same apparatus^{10,20,27}, where 300 K-based calculations were found to match experimental data well.

For simplicity we assume that the photodissociation cross section is independent of J and only thermalize the vibrational distribution. Assuming thermally-populated levels at $T = 300$ K, 81.6% and 10% of the population is in the $v=0$ and $v=1$ vibrational levels of the ground $\Omega=8$ potential, respectively. The only remaining level which is non-negligibly populated in thermal equilibrium is the $v=0$ vibrational level of the ground $\Omega=7$ potential, so we approximate all of the remaining 8.4% to be here in the

calculation. The spectroscopic constants for the ground $\Omega=8$ and 7 potentials are given in Table III.

The Franck-Condon principle states that the internuclear separation remains approximately unchanged during an electronic transition²⁸. In Fig. 1 this principle is illustrated by a vertical line at the peak internuclear separation of the $v = 0$ state, and employing the reflection approximation²⁹, we predict that photon energies between $37,500 \text{ cm}^{-1}$ and $44,500 \text{ cm}^{-1}$ will dissociate the DyCl^+ molecule.

In order to further quantify this process we have used the RCI-VB method to determine the electronic transition dipole moments. We find that their values range from $0.001ea_0$ to $0.2ea_0$ at the equilibrium separations of the $\Omega = 8$ and 7 attractive potentials, where e is the charge of the electron. Of the thirty-two repulsive $\Omega' = 6, 7, 8,$ and 9 potentials there are only fourteen potentials with transition dipole moments larger than $0.1ea_0$ that dissociate to the $\text{Dy}^+ + \text{Cl}$ limit. The seven excited potentials in the upper panel of Fig. 1 with a relatively large transition dipole moment to the $\Omega = 8$ ground state are highlighted in red, whereas the other seven potentials with large dipole moments to the ground $\Omega=7$ state are highlighted in blue.

The selectivity of the transition dipole moment follows from the ground and excited electronic wavefunctions. The wavefunction of the X state is dominated by the $\text{Dy}^{++} + \text{Cl}^-$ configuration, with its single active $4f^{10} \text{ Dy}^{++}$ shell with total core electron projection quantum number $\Omega_c = 8$, and more importantly with a closed $3p^6 \text{ Cl}$ valence shell and projection quantum number $\Omega_v = 0^+$, such that $\Omega = \Omega_c + \Omega_v$. The electronic wavefunction

v	$E_v/(hc) \text{ (cm}^{-1}\text{)}$		v	$E_v/(hc) \text{ (cm}^{-1}\text{)}$	
	$^{161}\text{Dy}^{35}\text{Cl}^+$	$^{161}\text{Dy}^{37}\text{Cl}^+$		$^{161}\text{Dy}^{35}\text{Cl}^+$	$^{161}\text{Dy}^{37}\text{Cl}^+$
0	-32351	-32356	15	-25854	-26413
1	-31914	-31928	16	-25435	-25590
2	-31495	-31518	17	-25019	-25182
3	-31077	-31110	18	-24605	-24777
4	-30648	-30692	19	-24192	-24373
5	-30205	-30260	20	-23780	-23970
6	-29752	-29818	21	-23367	-23566
7	-29295	-29372	22	-22955	-23163
8	-28841	-28926	23	-22543	-22760
9	-28398	-28491	24	-22133	-22359
10	-27968	-28069	25	-21725	-21958
11	-27543	-27652	26	-21319	-21560
12	-27119	-27238	27	-20916	-21164
13	-26697	-26825	28	-20516	-20772
14	-26275	-26413	29	-20120	-20382

TABLE II. The predicted binding energy of the first thirty vibrational energies of the lowest $n, \Omega = 1, 8$ or X potential of the $^{161}\text{Dy}^{35}\text{Cl}^+$ and $^{161}\text{Dy}^{37}\text{Cl}^+$ isotopes in the $J = 8$ rotational state.

TABLE III. $^{161}\text{Dy}^{35}\text{Cl}^+$ molecular spectroscopic constants for the deepest $\Omega = 7$ and 8 potentials

State	R_e [a_0]	D_e [cm^{-1}]	ω_e [cm^{-1}]	B_e [cm^{-1}]
$\Omega=8$	4.63	32	508	441
$\Omega=7$	4.63	32	273	466

for the optically-active repulsive states is controlled by interactions between the ^2S valence electron of the Dy^+ 6s shell and the ^2P hole of the Cl 2p^5 shell. An optical transition will excite an electron from the 3p^6 shell of Cl^- into the 6s shell of Dy^+ without affecting the 4f^{10} ($\Omega_c=8$) core. There are only a few one-electron transitions from the $\Omega=8$ ground state into repulsive excited states. In fact, selection rules suggest that only three $\Omega'=7$, one $\Omega'=8$, and three $\Omega'=9$ excited states have the same 4f^{10} core state as the initial $\Omega=8$ ground state. All other transitions are one or more orders of magnitude weaker, because they involve a change of state of two electrons. For the ground $\Omega=7$ potential a similar reasoning shows that only three $\Omega'=6$, one $\Omega'=7$, and three $\Omega'=8$ excited states have significant transition dipole moments.

Using the procedures described in Ref. 20 and a Hund's case (c) coupling scheme to describe the molecular rotation, we predict the photodissociation cross section as a function of laser frequency ν , and compare the results with experimental data, as presented in section (IV).

III. EXPERIMENTAL METHODS

The DyCl^+ photodissociation spectrum was recorded using an integrated ion trap and time-of-flight mass spectrometer (ToF-MS) system, shown in Fig. 2(a), which has been described in previous work^{27,30}. Here we provide an overview of the experimental setup and procedures, where particular attention is paid to details specific to this report, and refer the reader to the above Refs. for a more complete description of the apparatus.

A pressed, annealed pellet of DyCl_3 , situated ~ 3 cm away from the center of a linear quadrupole ion trap (LQT), is initially ablated by a single focused pulse from a 1064 nm Nd:YAG laser. The LQT, which has a field radius $r_0 = 7.92$ mm and an electrode radius $r_e = 3.18$ mm, operates at a frequency $\Omega_{\text{rf}} = 2\pi \times 375$ kHz, and is switched on ~ 50 μs after the ablation pulse. Non-linear motional resonances in the secular ion motion are exploited in order to reduce trapped species from the initial ablation yield other than DyCl^+ , the most prominent of which is DyOH^+ , as described in the following. The initial trapping amplitude $V_{\text{rf}} = 78$ V, which corresponds to a Mathieu- q parameter for DyCl^+ (isotopic average mass $m = 197$ amu) of $q = 4eV_{\text{rf}}/(mr_0^2\Omega_{\text{rf}}^2) = 0.44$. At this V_{rf} , the trap drives nonlinear resonant motion³¹ in Dy^+ ions, thus making them unstable (and therefore ab-

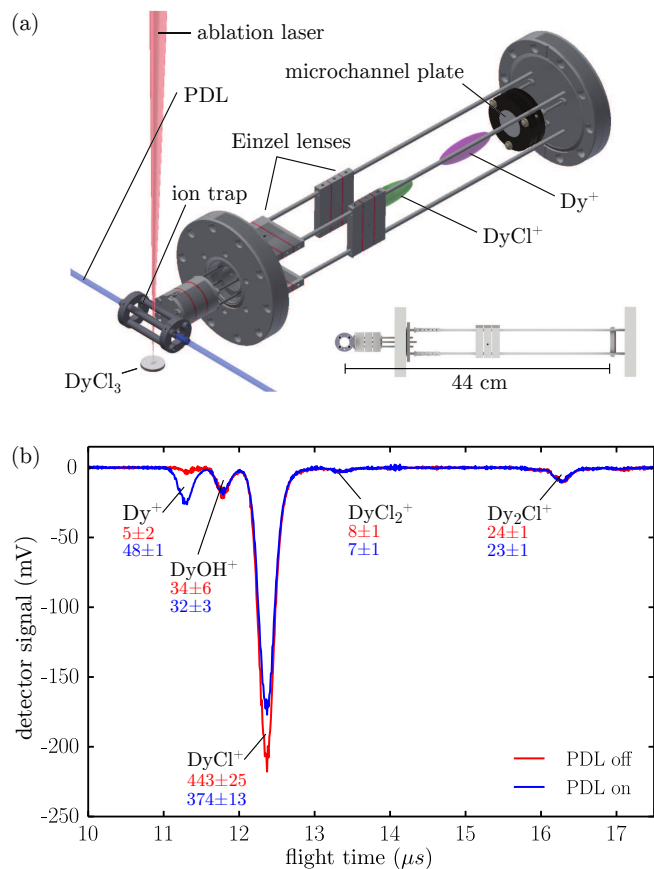


FIG. 2. (a) A 3-D rendering of the ion trap and ToF-MS apparatus, with an artist's impression of species in the drift tube, separated due to their different masses. (b) Typical time-of-flight mass spectrometer traces used to determine the photodissociation yield, where dips represent arrival of ions at the detector. The measured number of ions in each peak is given underneath the species name, and the PDL wavenumber is ~ 45000 cm^{-1} .

sent after several rf cycles) upon initial capture of the ablation products. After approximately 300 ms, V_{rf} is ramped over 200 ms to 85 V, where a nonlinear motional resonance in DyOH^+ is driven. After 800 ms at this trapping amplitude, most of the DyOH^+ has escaped the trap, and only DyCl^+ ions and heavier (Dy_2Cl^+ is the only significant contributor) remain. The voltage is then ramped down over 200 ms to $V_{\text{rf}} = 65$ V, where Dy_2Cl^+ is less prominent due to the lower mass-dependent trap depth $D_r \propto 1/m$, yet both Dy^+ and DyCl^+ (for which $q = 0.364$) are stable. There remains a small background of Dy^+ , DyOH^+ and Dy_2Cl^+ after mass filtering; an average Dy^+ background was measured, and incorporated into the resulting photodissociation yields; and tests show that DyOH^+ and Dy_2Cl^+ do not photodissociate at the photon energy range considered here.

Once the loading and mass filtering stages are complete, 1.7 s after ablation, the DyCl^+ is illuminated by laser pulses, propagating along the LQT axis, from a pulsed dye laser (PDL) operating with pulse duration

$\tau_p \sim 10$ ns, pulse energy $E_p \sim 0.5$ mJ, and repetition rate $f_{\text{rep}} = 10$ Hz, for $t = 1.3$ s.

The PDL beam is expanded by a telescope at the output of the laser, and subsequently passed through two sequential irises, each with an aperture of radius $r = 1.5$ mm, to ensure uniform intensity distribution across the ion cloud, whose mean radius at the expected maximum translational temperature, 3400 K, is predicted to be ~ 1.2 mm.

After the PDL pulses have been applied, the ions are radially ejected from the LQT into the ToF-MS. Ejection is achieved by switching off the trapping rf field and simultaneously applying 2 kV and 1.8 kV DC respectively, with < 1 μs rise-time, to the LQT electrode pairs furthest from and closest to the entrance to a 44 cm drift tube. To maximise signal, focussing of the in-flight ions is performed using Einzel lenses; and the ions are detected upon arrival at a microchannel plate. Fig. 2(b) shows typical ToF-MS signals with and without the PDL (extraction occurs after the same trapping duration for both cases), where the dips represent arrival of ions. The ToF-MS Dy^+ arrival time is calibrated by trapping and ejecting the Dy^+ ablation yield from a 99.9 % pure Dy ingot, and we fit the remaining arrival times observed from the ablation of DyCl_3 according to $t = A\sqrt{m} + t_0$, where t_0 is a time offset imposed by the pulsing electronics, and A is a constant determined by the pulse characteristics and flight-tube length. By minimising the χ^2 statistic, we predict the peak at around 11.8 μs to be DyOH^+ and not DyO^+ , although it is important to note that the resolution afforded by the ToF-MS for species at 300 K is insufficient to discriminate between these masses with complete certainty. To improve the ToF-MS resolution, one may employ laser cooling techniques to increase phase-space density, as described in Ref. 32. As betrayed in Fig. 2(b), small amounts of DyOH^+ , Dy_2Cl^+ , and DyCl_2^+ are present in the ion trap even after mass filtering, yet, fortuitously, these species did not detectably photodissociate at the photon energies considered here. Furthermore, our data demonstrate that DyOH^+ is not formed due to reactions between the Dy^+ produced during photodissociation of DyCl^+ and any background of water (or oxygen if the species is in fact DyO^+) at a detectable level. Our DyCl^+ sample consists of all naturally-abundant isotopes of the molecule, yet we consider only $^{161}\text{Dy}^{35}\text{Cl}^+$ for calculation purposes, since the isotope shift of the photodissociation cross section is expected to be negligible on the photon energy scales considered here.

From the ToF-MS traces, we infer the photodissociation cross section σ at wavenumber ν according to

$$\sigma = \frac{hc\nu}{\bar{I}t} \ln\left(\frac{1}{1-\eta}\right) \quad (1)$$

where h is Planck's constant, c is the speed of light, $\bar{I} = f_{\text{rep}}E_p/\pi r^2$ is the time-averaged intensity of the PDL

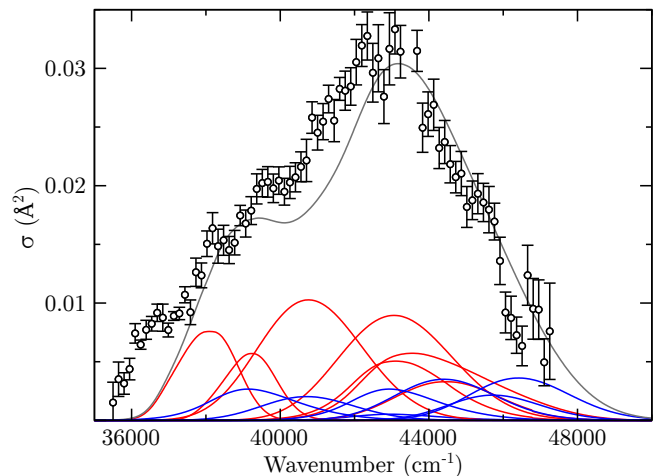


FIG. 3. (color online) The experimental (markers) and theoretical (grey line) thermalized photodissociation cross section of DyCl^+ molecular ions as a function of photon wavenumber ν/c . The theoretical curves are for $^{161}\text{Dy}^{35}\text{Cl}^+$ at $T = 300$ K. The red and blue lines show partial contributions to the cross section due to transitions from vibrational levels of the $\Omega = 8$ and 7 ground state potentials, respectively. These colors correspond to those used in Fig. 1.

beam, and

$$\eta = \frac{N[\text{Dy}^+] - N_{\text{BG}}[\text{Dy}^+]}{(N[\text{Dy}^+] - N_{\text{BG}}[\text{Dy}^+]) + N[\text{DyCl}^+]} \quad (2)$$

is the fractional photodissociation yield, in which $N[\text{S}]$ is the measured number of species S arriving at the ion detector, and the BG subscript denotes the average background number, as measured with the PDL switched off.

A total of six different dye solutions including one exalite and five coumarin based dyes were used to span the range $35,500 \leq \nu \leq 47,400$ cm^{-1} with intervals of 50 cm^{-1} , where 10 measurements of η were taken at each sampled ν . The PDL pulse energy E_p was recorded for every pulse. Above $\nu \sim 46,000$ cm^{-1} , PDL output energies began to decrease, and attenuation of the pulses en-route to the LQT by both air and optics became increasingly apparent, leading to reduced signal-to-noise. Statistical error on the measurement of σ arises due to shot-to-shot fluctuations in E_p , along with variations in η .

IV. RESULTS & DISCUSSION

Fig. 3 shows a comparison of our experimental and theoretical photodissociation cross sections. The markers represent the data, which are binned and averaged with bin widths of 150 cm^{-1} , and their error bars represent the standard error within each bin. The theoretical cross section has an unresolved double-peaked structure with a maximum around a photon energy of 43,000 cm^{-1} and includes contributions from fourteen dominant transitions

from the thermally populated $\Omega=8$ and 7 states and their corresponding $v=0$ and 1 levels. The maximum of the data approximately coincides with that of the predicted cross section. The data do not clearly reveal the predicted double-peaked structure, yet they exhibit structure around $39,000\text{ cm}^{-1}$ which might represent the predicted smaller peak. We find that the data lie mostly above the predicted curve at photon energies below $43,000\text{ cm}^{-1}$, and above this value they agree well with the prediction. There appears to be structure around $36,500\text{ cm}^{-1}$ present in the experiment but not in the theoretical prediction, which might point toward the existence of repulsive states whose energies are lower at the vertical transition turning point (illustrated by the dashed line in Figure 1) than those calculated here. Nevertheless, the agreement between experiment and theory is satisfactory given the accuracy of the potentials and dipole moments as well as the approximations made in evaluation of the cross section. It is important to note that no scaling was applied to parameters in the calculation for purposes of achieving a good match with the data.

Although calculations of molecular potentials have in this work been restricted to those corresponding to the four lowest-energy dissociation limits, we may speculate regarding the position of bound excited molecular potentials in DyCl^+ . For the purposes of laser cooling and quantum information experiments, we are particularly interested in the existence of electronic transitions which have optical frequencies and highly diagonal Franck-Condon factors (FCFs). For lanthanide-halides, it is generally expected that transitions involving the promotion of $4f$ or $6s$ electrons on the metal ion to $5d$ or $6p$ orbitals significantly affect the bonding characteristics of the molecule³³, thus leading to FCFs which are non-diagonal in nature. On the other hand, intra-shell $f-f$ excitations within the $\text{Dy}^{++}[4f^{10}]$ metal core (see Ref. 34 for free Dy^{++} spectra) are not expected to affect the molecule's bonding characteristics, owing to the submerged nature of the $4f$ shell, as discussed in the context of lanthanide-trihalides in Ref. 22. Such transitions are commonly exploited in Lanthanide-ion-doped solid-state laser materials, such as $\text{Nd}^{3+}[4f^3(^4F_{11/2} \leftarrow ^4I_{3/2})]$ in $\text{Nd}^{3+}:\text{YAG}$ crystals, where vibrations and interactions with ligand fields lift the Laporte (parity) selection rule, leading to sharp spectral lines²³. In free Dy^{++} , transitions within the $4f^{10}(^5I)$ core ground configuration, whose states should be slightly mixed, would occur in the near-infrared frequency range³⁴, with the largest interval being $11,014\text{ cm}^{-1}$ for $4f^{10}(^5I_8 \leftarrow ^5I_4)$. With parity mixing induced by the ligand field in $\text{Dy}^{++}\text{Cl}^-$, it is expected that these $f-f$ transitions will be strengthened. Should this be the case, we would expect a manifold of NIR-addressable, bound, excited potentials, whose equilibrium internuclear separations r_e are close to that of the ground state. Such transitions, while narrow, would exhibit diagonal FCFs, thus potentially making them amenable to narrow-line laser cooling and coherent quantum manipulation. As such, they will form the basis for

future work on DyCl^+ .

V. SUMMARY

We have computed and measured the photodissociation cross section of DyCl^+ for photon energies between $35,500\text{ cm}^{-1}$ and $47,500\text{ cm}^{-1}$. Calculations show that there are 108 potential curves that dissociate to lowest spin-orbit ground states of Dy^+ and Cl , which highlights the complex role played by the open $4f^{10}$ shell of Dy^+ . Only nine of these potentials are attractive and correspond to the “ionically” bonded $\text{Dy}^{++}\text{Cl}^-$, where the outer $6s$ electron of Dy has transferred into the $\text{Cl } 2p^5$ shell. All other potential curves corresponding to these dissociation limits are repulsive. Our experimental photodissociation cross section, obtained using an integrated ion trap and time-of-flight mass spectrometer, is found to agree satisfactorily with the calculations, given the myriad repulsive potentials and approximations made in the predicted transition moments. We observe a broad, asymmetric photodissociation cross section peaked at around $43,000\text{ cm}^{-1}$, which is well-represented by calculations assuming thermally populated internal molecular states. Future work will aim to probe the existence of optically-addressable, vertical $f-f$ transitions in the molecule, towards its use in laser cooling, ultracold chemistry, and quantum information experiments.

VI. ACKNOWLEDGEMENTS

AD acknowledges valuable discussions with Michael Heaven of Emory University. This work was supported by National Science Foundation (NSF, grant Nos. PHY-1205311, PHY-1308573), Army Research Office (MURI-ARO, grant Nos. W911NF-15-1-0121, W911NF-14-1-0378), and Air Force Office of Scientific Research (AFOSR, grant No. FA-14-1-0321) grants.

- ¹L. D. Carr, D. DeMille, R. V. Krems, and J. Ye, *New Journal of Physics* **11**, 055049 (2009).
- ²D. I. Schuster, L. S. Bishop, I. L. Chuang, D. DeMille, and R. J. Schoelkopf, *Physical Review A* **83**, 012311 (2011).
- ³L. F. Pařteka, A. Borschevsky, V. V. Flambaum, and P. Schwerdtfeger, *Physical Review A* **92**, 012103 (2015).
- ⁴E. Meyer, J. Bohn, and M. Deskevich, *Physical Review A* **73**, 062108 (2006).
- ⁵A. Leanhardt, J. Bohn, H. Loh, P. Maletinsky, E. Meyer, L. Sinclair, R. Stutz, and E. Cornell, *Journal of Molecular Spectroscopy* **270**, 1 (2011).
- ⁶S. J. Yun and C. H. Nam, *Physical Review A - Atomic, Molecular, and Optical Physics* **87**, 040302 (2013).
- ⁷K. Mø lhave and M. Drewsen, *Physical Review A* **62**, 011401 (2000).
- ⁸A. Ostendorf, C. Zhang, M. Wilson, D. Offenber, B. Roth, and S. Schiller, *Physical Review Letters* **97**, 243005 (2006).
- ⁹A. K. Hansen, O. O. Versolato, L. Kosowski, S. B. Kristensen, A. Gingell, M. Schwarz, A. Windberger, J. Ullrich, J. R. C. López-Urrutia, and M. Drewsen, *Nature* **508**, 76 (2014).
- ¹⁰W. G. Rellergert, S. T. Sullivan, S. J. Schowalter, S. Kotochigova, K. Chen, and E. R. Hudson, *Nature* **495**, 490 (2013).

- ¹¹R. J. Saykally and R. C. Woods, *Annual Review of Physical Chemistry* **32**, 403 (1981).
- ¹²E. Shenyavskaya and L. Gurvich, *Journal of Molecular Spectroscopy* **81**, 152 (1980).
- ¹³W. J. Balfour and B. Lindgren, *Physica Scripta* **22**, 36 (1980).
- ¹⁴D. A. Ramsay and P. J. Sarre, *Journal of the Chemical Society, Faraday Transactions 2* **78**, 1331 (1982).
- ¹⁵A. Merer, A.-C. Cheung, and A. Taylor, *Journal of Molecular Spectroscopy* **108**, 343 (1984).
- ¹⁶A. Chanda, W. C. Ho, F. W. Dalby, and I. Ozier, *The Journal of Chemical Physics* **102**, 8725 (1995).
- ¹⁷A. Wüest and F. Merkt, *The Journal of chemical physics* **120**, 638 (2004).
- ¹⁸V. Goncharov and M. C. Heaven, *The Journal of chemical physics* **124**, 64312 (2006).
- ¹⁹J. M. Merritt, V. E. Bondybey, and M. C. Heaven, *The Journal of chemical physics* **130**, 144503 (2009).
- ²⁰K. Chen, S. J. Schowalter, S. Kotochigova, A. Petrov, W. G. Rellergert, S. T. Sullivan, and E. R. Hudson, *Physical Review A* **83**, 030501 (2011).
- ²¹I. O. Antonov and M. C. Heaven, *The journal of physical chemistry. A* **117**, 9684 (2013).
- ²²G. Lanza, Z. Varga, M. Kolonits, and M. Hargittai, *The Journal of chemical physics* **128**, 074301 (2008).
- ²³M. Hatanaka and S. Yabushita, *Theoretical Chemistry Accounts* **133**, 1517 (2014).
- ²⁴S. Kotochigova and E. Tiesinga, *The Journal of chemical physics* **123**, 174304 (2005).
- ²⁵I. S. Lim, P. Schwerdtfeger, B. Metz, and H. Stoll, *The Journal of chemical physics* **122**, 104103 (2005).
- ²⁶F. Weigend and R. Ahlrichs, *Physical chemistry chemical physics : PCCP* **7**, 3297 (2005).
- ²⁷P. Puri, S. J. Schowalter, S. Kotochigova, A. Petrov, and E. R. Hudson, *The Journal of chemical physics* **141**, 014309 (2014).
- ²⁸G. Herzberg, *Molecular Spectra and Molecular Structure* (D. van Nostrand company, Inc, 1957).
- ²⁹H. Lefebvre-Brion and R. W. Field, *The Spectra and Dynamics of Diatomic Molecules* (Elsevier, 2004) pp. 469–549.
- ³⁰S. J. Schowalter, K. Chen, W. G. Rellergert, S. T. Sullivan, and E. R. Hudson, *The Review of scientific instruments* **83**, 043103 (2012).
- ³¹D. M. Eades, J. V. Johnson, and R. A. Yost, *Journal of the American Society for Mass Spectrometry* **4**, 917 (1993).
- ³²C. Schneider, S. J. Schowalter, K. Chen, S. T. Sullivan, and E. R. Hudson, *Physical Review Applied* **2**, 034013 (2014).
- ³³J. K. Gibson, *The Journal of Physical Chemistry A* **107**, 7891 (2003).
- ³⁴N. Spector, J. Sugar, and J.-F. Wyart, *Journal of the Optical Society of America B* **14**, 511 (1997).